His/Met heme ligation in the PioA outer membrane cytochrome enabling light-driven extracellular electron transfer by *Rhodopseudomonas palustris* TIE-1.

Dao-Bo Li[1#], Marcus J. Edwards[1]*, Anthony W. Blake[1], Simone E. Newton-Payne[1], Samuel E. H. Piper[1], Leon P. Jenner[1], Katarzyna P. Sokol[2$], Erwin Reisner[2], Jessica H. van Wonderen[1], Thomas A. Clarke[1]* and Julea N. Butt[1]*

From the [1]School of Chemistry and School of Biological Sciences, University of East Anglia, Norwich Research Park, Norwich, NR4 7TJ, UK; [2] Department of Chemistry, University of Cambridge, Lensfield Road, Cambridge CB2 1EW, UK

[#] Present address: Guangdong Provincial Key Laboratory of Microbial Culture Collection and Application, Guangdong Institute of Microbiology, Guangdong Academy of Sciences, Guangzhou, China and State Key Laboratory of Applied Microbiology Southern China, Guangzhou, China.
[$] Present address: Electrochemical Materials Laboratory, Dept. of Materials Science and Engineering, Massachusetts Institute of Technology, 77 Massachusetts Ave., Cambridge, MA 02139.

*To whom correspondence should be addressed: Julea Butt: School of Chemistry, University of East Anglia, Norwich Research Park, Norwich, NR4 7TJ, UK. j.butt@uea.ac.uk, Tel. (44) 1603 593877; Fax. (44) 1603 592003. Thomas Clarke: School of Biological Sciences, University of East Anglia, Norwich Research Park, Norwich, NR4 7TJ, U.K tom.clarke@uea.ac.uk, Tel. (+44) 1603 2190; Fax (+44) 1603 592250. Marcus Edwards: School of Biological Sciences, University of East Anglia, Norwich Research Park, Norwich, NR4 7TJ, U.K m.edwards@uea.ac.uk, Tel. (+44) 1603 592269; Fax (+44) 1603 592250.

Abbreviations: MR-1, *Shewanella oneidensis* MR-1; SDS-PAGE, sodium dodecyl sulphate - polyacrylamide gel electrophoresis; SHE, Standard Hydrogen Electrode.

ABSTRACT

A growing number of bacterial species are known to move electrons across their cell envelopes. Naturally this occurs in support of energy conservation and carbon-fixation. For biotechnology it allows electron exchange between bacteria and electrodes in microbial fuel cells and during microbial electrosynthesis. In this context *Rhodopseudomonas palustris* TIE-1 is of much interest. These bacteria respond to light by taking electrons from their external environment, including electrodes, to drive CO_2-fixation. The PioA cytochrome, that spans the bacterial outer membrane, is essential for this electron transfer and yet little is known about its structure and electron transfer properties. Here we reveal the ten *c*-type hemes of PioA are redox active across the window +250 to -400 mV *versus* Standard Hydrogen Electrode and that the hemes with most positive reduction potentials have His/Met and His/H_2O ligation. These chemical and redox properties distinguish PioA from the more widely studied family of MtrA outer membrane decaheme cytochromes with ten His/His ligated hemes. We predict a structure for PioA in which the hemes form a chain spanning the longest dimension of the protein, from Heme 1 to Heme 10. Hemes 2, 3 and 7 are identified as those most likely to have His/Met and/or His/H_2O ligation. Sequence analysis suggests His/Met ligation of Heme 2 and/or 7 is a defining feature of decaheme PioA homologs from over 30 different bacterial genera. His/Met ligation of Heme 3 appears to be less common and primarily associated with PioA homologs from purple non-sulphur bacteria belonging to the alphaproteobacteria class.

INTRODUCTION

Iron is an abundant component of marine, freshwater and subsurface habitats where the Fe(III)/(II) reduction potential has values between approx. -300 and +800 mV *versus* Standard Hydrogen Electrode (SHE) [1]. This property, arising from the different iron coordination spheres of its mineral and complexed forms, benefits the numerous microorganisms able to harness this couple for energy metabolism [1-5]. Examples are found in the reduction of Fe(III) that terminates anaerobic respiratory electron transfer chains in dissimilatory iron reducers, and in the oxidation of Fe(II) providing electrons for CO_2-fixation by lithoautotrophic iron oxidisers. To use the Fe(III)/(II) transition in these ways, the corresponding organisms have evolved to manage the insolubility of Fe(III) at circum-neutral pH [6]. Lithoautotrophs avoid the formation of intracellular Fe(III) precipitates by catalysing Fe(II) oxidation on the cellular surface. Mineral forms of Fe(III) are reduced for anaerobic respiration when dissimilatory iron reducers move electrons to the cell surface. Both strategies rely on electron exchange across the cell envelope to couple the redox activities of intracellular enzymes with extracellular iron.

For several species of dissimilatory iron reducing Gram-negative bacteria, genetic and biochemical studies have demonstrated a defining role for porin:cytochrome complexes in electron transfer across the outer membrane lipid bilayer [4, 7-10]. The first molecular structure for such a complex was very recently resolved [11] and this revealed an insulated biomolecular wire for the MtrA:MtrB complex from *Shewanella baltica* OS185 (Figure 1A left). At the core of that complex is a chain of ten close-packed *c*-

hemes. This heme chain spans the lipid bilayer allowing complementary Fe(III) ↔ Fe(II) transitions of neighbouring sites to transfer electrons from the periplasm to the cell exterior. All ten hemes have His/His ligation provided by MtrA residues and they are covalently linked to CxxCH *c*-heme binding amino acid motifs in the same protein. MtrB is a β-barrel porin that forms a sleeve round MtrA. MtrB confers solubility in the hydrophobic membrane interior and precludes hemes in the centre of the MtrA wire from undergoing interprotein electron transfer.

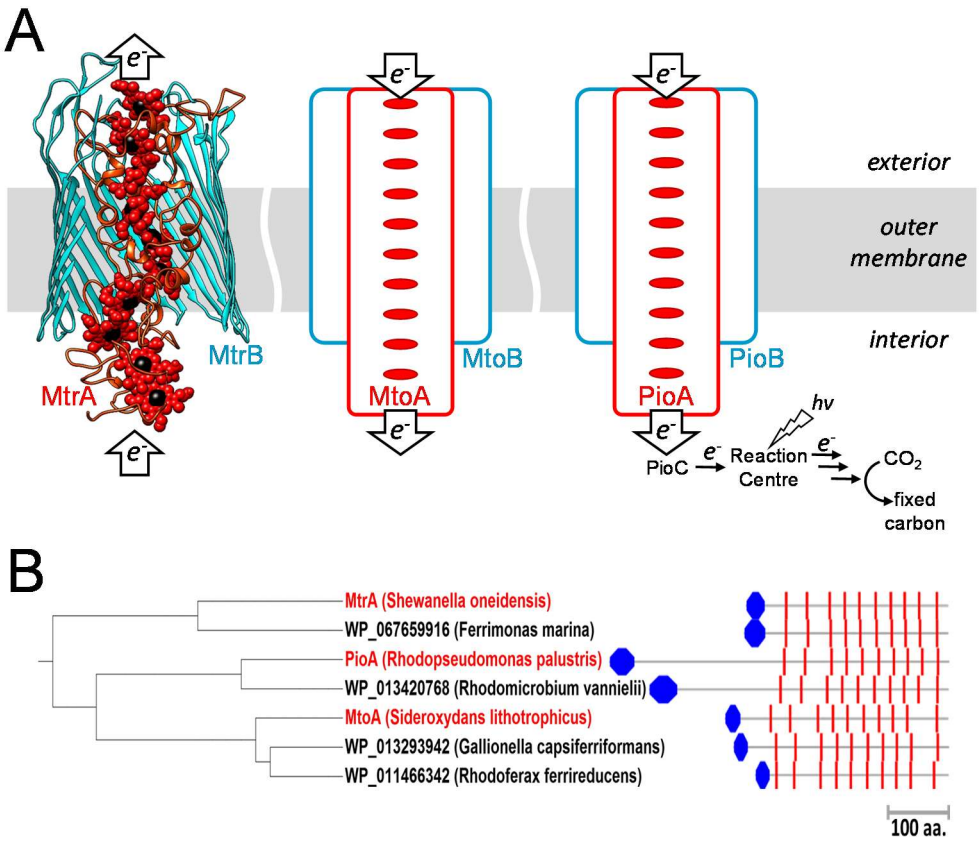

Figure 1. *R. palustris* PioA homologs. (A) *S. baltica* OS185 MtrAB (left, (11)) highlighting the MtrA with 10 *c*-type hemes (red spheres with Fe black) running through the MtrB barrel by omission of beta-strands on the front face of MtrB. Schematic of *S. lithotrophicus* MtoAB (centre) and *R. palustris* PioAB (right). Large arrows indicate the direction of natural electron transfer through each complex, see text and (6) for details. For PioAB the proposed intracellular electron transfer pathway for carbon-fixation is illustrated (see [12] for details). **(B)** Cladogram of *R. palustrus* PioA homologs. Amino acid sequences and their relative lengths are indicated by grey lines aligned at the C-terminus. The locations of *c*-type heme binding motifs (CxxCH) are indicated as red bars and the predicted N-terminal Sec signal peptides are shown as blue octagons. Branches are labelled either with protein name or RefSeq protein accession code with the bacterial species given in parentheses. Branches corresponding to MtrA (*S. oneidensis*), PioA (*R. palustris*) and MtoA (*S. lithotrophicus*) are indicated with red labels.

The *mtrA-mtrB* genes are co-transcribed and highly conserved across all species of *Shewanella* [13]. Close homologs of the *mtrA-mtrB* genes are also found in Fe(II) oxidisers [4]. These genes, termed *mtoA-mtoB*, for species of *Sideroxydans*, *Gallionella*, *Thiomonas*, *Dechloromonas*, and *Rhodomicrobium* are predicted to yield outer membrane porins (MtoB) into which decaheme cytochromes (MtoA, Figure 1B) may be embedded (Figure 1A centre). In accord with this hypothesis, expression of *mtoA*, an *mtrA* homolog from *Sideroxydans lithotrophicus* ES-1, partially restored ferrihydrite reduction by *Shewanella oneidensis* MR-1 lacking genomic *mtrA* [9].

Homologs of the *Shewanella mtrA-mtrB* genes are also found in *Rhodopseudomonas palustris* TIE-1 [14, 15] and *Rhodomicrobium vannielii* [4] where they are termed *pioA-pioB*. The *pio* gene products allow phototrophic Fe(II)-oxidation (Figure 1A right), giving insight into an ancient form of photosynthesis, and supporting light-driven CO_2-fixation coupled to cathodic electron influx [12, 16-18]. An outer membrane porin of ~800 amino acids similar to MtrB is predicted from *pioB*. The predicted gene product from *pioA* is larger than MtrA, ~540 and 300 residues respectively (Figure 1B). However post-secretory proteolysis of the PioA N-terminus results in a mature functional cytochrome of similar size to MtrA [14, 19]. Here we present the first detailed description of the structure-function relationship for PioA. Spectroscopic, redox and structural properties of PioA are described and found to differ from the corresponding properties of the well-studied MtrA proteins [7, 11]. The results provide molecular insight into differences between homologous proteins that have evolved to move electrons in to or out from bacteria, PioA and MtrA respectively.

RESULTS

Purification of PioA as a monomeric 40 kDa decaheme cytochrome. Heterologous production of several different multiheme cytochromes in MR-1 has been achieved with pBAD202 plasmids allowing expression from an L-arabinose inducible promoter [20-22]. As *R. palustris* TIE-1 is a slow growing organism that reaches very low biomass compared to MR-1 [14, 19, 23], we investigated the latter organism for heterologous production of PioA. As described in Experimental Procedures, pBAD202 was engineered to carry the codon optimized *R. palustris* TIE-1 *pioA* gene with a 3' extension encoding for a C-terminal Strep-II affinity tag (Figure S2, S3) to facilitate protein purification. The resulting plasmid, pBAD202_*pioA* was introduced into MR-1 by electroporation.

Cells were induced through the addition of 5 mM L-arabinose in the mid-exponential phase of growth and harvested approx. 6 hr later. Sodium dodecyl sulphate -polyacrylamide gel electrophoresis (SDS-PAGE) of the lysed cells combined with heme staining (Figure 2A) revealed a *c*-type cytochrome migrating with an apparent mass of approx. 30 kDa which was not detected in equivalent analysis of non-induced cells, or MR-1 lacking the pBAD202_*pioA* plasmid. The identified cytochrome was confirmed as the major Strep-II tagged protein of arabinose induced cells when it was purified from the cell lysate by affinity chromatography (Figure 2B).

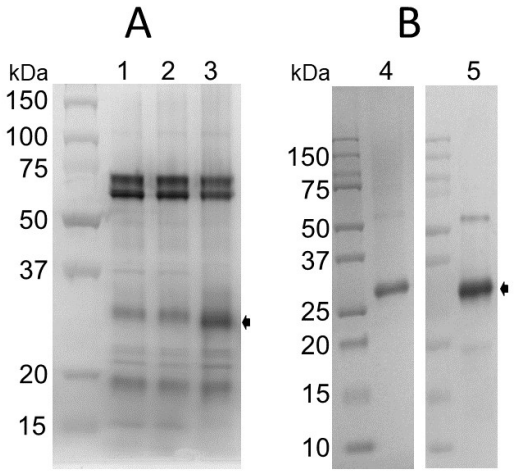

Figure 2. Heterologous production of PioA in MR-1. (A) SDS-PAGE gels with proteins visualized by peroxidase-linked heme stain for cells of MR-1 (lane 1), cells of MR-1 carrying the pBAD202_*pioA* plasmid (lane 2) and arabinose induced cells of MR-1 carrying the pBAD202_*pioA* plasmid (lane 3). **(B)** SDS-PAGE with proteins visualized by Coomassie (lane 4) and peroxidase-linked heme stain (lane 5) for samples of PioA purified from arabinose induced cells of MR-1 carrying the pBAD202_*pioA* plasmid. Molecular weight markers as indicated. Arrows indicate the position of the band corresponding to PioA.

The purified protein had a red colour and the electronic absorbance, described below, was dominated by features characteristic of *c*-type hemes. Because all Cys residues encoded by *pioA* occur in the ten CxxCH heme-binding motifs, thiol(ate) content was analysed as an indicator of *c*-heme loading. If 10 conventional *c*-type hemes are present there will be no free thiol(ate) groups as all ten Cys sidechains will be present as thioether bonds to the corresponding hemes. A colorimetric assay revealed significantly less than 1 thiol(ate) per peptide, (e.g. Figure S4) from which it was concluded that purified PioA contained 10 *c*-type hemes.

LC-MS revealed a homogeneous sample with an experimental mass of 39 966.4 Da. A mass of 39 963.6 Da was predicted for the Strep-II tagged decaheme PioA with Ala243 as the N-terminal residue (Figure S3) using Compute PI/Mw (https://web.expasy.org/compute_pi) and assuming each covalently attached heme would contribute 615.17 Da. This description of the mature cytochrome is in agreement with a recent study [19] that identified Ala243 as the N-terminal residue of PioA purified from *R. palustris* TIE-1. The extinction coefficient for oxidised PioA at 407 nm was calculated as 1440 mM^{-1} cm^{-1} using the pyridine-hemochrome method [24].

An assessment of the properties of PioA in solution was made using analytical centrifugation. Sedimentation equilibrium analysis at two PioA concentrations (0.5 and 5 μM) was performed at three centrifugation speeds (15k, 18k and 21k rpm) and the absorbance profiles (Figure 3A and Figure S5) were

well-described by the behaviour predicted for a single, non-interacting species with a weight average molecular mass of 45.5 ± 0.2 kDa. Comparing this value to the results of LC-MS indicate that PioA is a monomer under the experimental conditions. PioA (0.8 μM) was also analysed by sedimentation velocity analysis through repeated measurement of the absorbance during centrifugation at 40k rpm (Figure 3B). The absorbance profiles were fitted using the Lamm equation [25] providing a single peak in the *c*(s) distribution (Figure 3B) that is characteristic of a homogenous sample containing a single species. That species is described by a sedimentation coefficient of 2.94 S and a diffusion coefficient of 6.48×10^{-7} cm^2 s^{-1} from which a molecular weight of 43.2 kDa is calculated using the Svedberg equation as described in *Experimental Procedures*. Thus, sedimentation velocity analysis is also indicative of monomeric PioA. From the measured sedimentation coefficient and molecular weight, an f/f_0 ratio of 1.344 was calculated. This ratio provides a comparison of the PioA frictional coefficient, f, to that of a perfect sphere of equal mass, hydration and viscosity, f_0, and is indicative of a prolate or oblate elliptical protein molecule with an elongated axis.

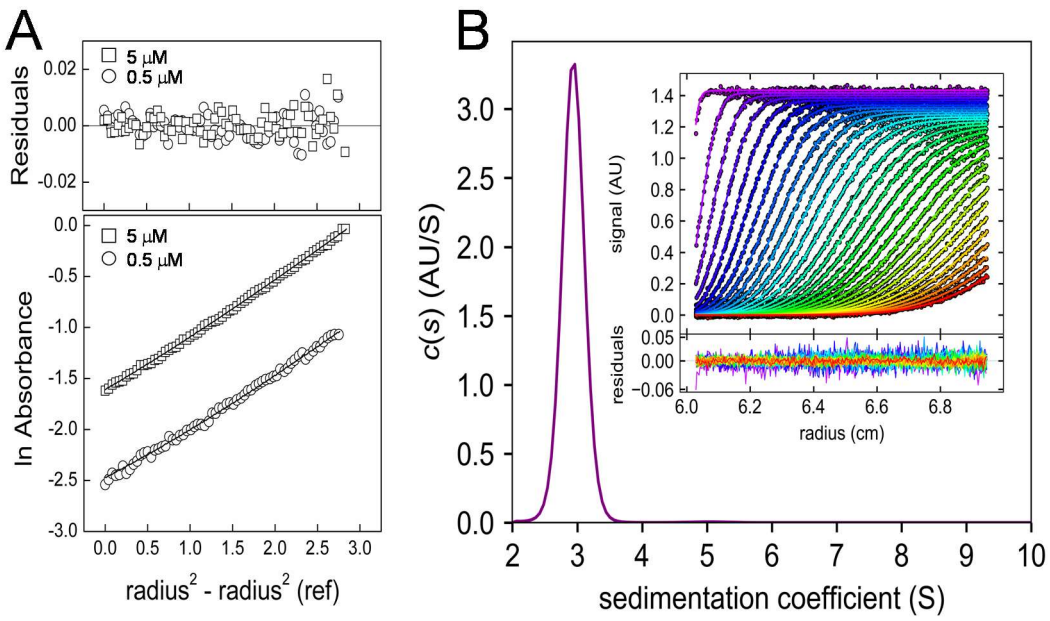

Figure 3. Hydrodynamic analysis of PioA. (A) Sedimentation equilibrium analysis of PioA for protein concentrations of 0.5 μM (circles) and 5 μM (squares) at 15k rpm. Lines are fitted to the experimental data using a non-interacting, single-component model with a molecular weight of 45 kDa. Upper panel shows residual difference between the experimental and fitted data. (**B**) Inset: Sedimentation velocity analysis of 0.8 μM PioA monitored by absorbance at 409 nm (markers) and fit (lines) to the Lamm equation with residual absorption from the fitted data shown in the lower panel. The fitted *c*(s) distribution of sedimentation coefficients indicates the presence of only monomeric species.

PioA is redox active between +250 and -400 mV *versus* SHE. Spectro-electrochemistry and cyclic voltammetry were used to study the redox properties of PioA at pH 7.4. For the former method, PioA was adsorbed on optically transparent mesoporous nanocrystalline SnO_2 electrodes [26]. Heme oxidation state was resolved by electronic absorbance spectroscopy after equilibrating the protein at numerous electrode potentials (Figure 4A). When poised at +250 mV *versus* SHE the spectrum revealed features characteristic of low-spin *c*-type heme in the Fe(III) state. The Soret band had maximum intensity at 407 nm and a broad lower intensity α/β-band was present between 500 and 600 nm. Spectroscopic features indicative of reduced heme appeared after equilibrating the adsorbed protein below approx. +200 mV, namely, a Soret band with maximum intensity at 419 nm and sharp α/β-bands at 552 and 523 nm respectively. Below approx. -400 mV the spectra indicated complete reduction of the protein.

Plotting the extent of PioA reduction as a function of equilibration potential (Figure 4A) suggests the majority of PioA hemes are reduced between approx. -100 and -300 mV and that 1 or 2 hemes are reduced between approx. +200 and -100 mV. However, confident deconvolution of these contributions is precluded because the spectral contribution of each heme is unknown. Therefore, a complementary view of PioA redox chemistry was sought from cyclic voltammetry. In this method each redox active site undergoing a single-electron (n = 1) process makes an equal contribution to the peaks resolved for oxidation, and reduction, of the adsorbed protein. The relatively large irregular charging currents measured with optically transparent SnO_2 electrodes, e.g. [27], prevented confident analysis of the peaks describing redox transformation of adsorbed PioA. However, clear well-defined peaks (Figure 4B) defining PioA redox activity were measured during cyclic voltammetry of the protein adsorbed on three-dimensional hierarchically-structured indium tin oxide electrodes [28, 29].

The areas of the peaks for PioA oxidation (positive current) and reduction (negative current) were equal, indicating reversible redox transformation of the protein. Both features describe redox activity between ≈ +250 and -400 mV, the same range for which spectro-electrochemistry revealed conversion of PioA between the deca-Fe(III) and deca-Fe(II) states. Maximum currents were detected at approx. -180 mV and a shoulder on the low potential flank together with a smaller well-defined shoulder on the high potential flank reveal contributions from hemes having several different reduction potentials. We assessed how well the peaks are described by the sum of ten equal contributions from isolated sites undergoing reversible n = 1 processes using the protocol of Doyle *et al* [30]. Both peaks are well-described by our choice of model (Figure 4B). Reduction potentials (± 15 mV) of +130, +45, -40, -40, -70, -100, -130, -165, -205 and -255 mV *versus* SHE are defined as the average values from fits to the oxidative and reductive peaks. We note that there are no indications of sharper features in the measured peaks that would indicate cooperative, e.g. n = 2, redox processes.

The redox properties of PioA change very little between pH 6.4 and 9.4 (Figure S6). This behaviour suggests that proton-coupled electron transfer over this pH range is less prevalent in PioA than other multiheme cytochromes [31, 32].

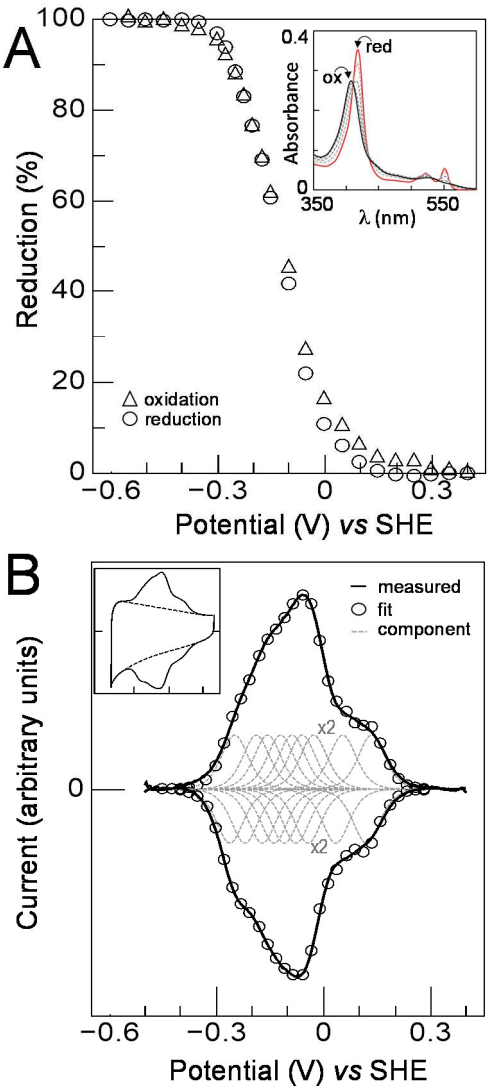

Figure 4. Redox activity of PioA. (A) Potentiometric titration of PioA adsorbed on SnO_2 electrodes for reduction (circles) and oxidation (triangles). Inset: Spectra at -0.6 (red), -0.2, -0.1, 0 (grey) and +0.4 V (ox, black). **(B)** Cyclic voltammetry of PioA adsorbed on a hierarchical indium tin oxide electrode (continuous line) together with a fit (circles) to the sum of ten equal contributions (broken lines) from independent $n = 1$ centres. For details of the fit see text. Note: contributions with the same reduction potentials (×2) give the impression of only nine contributions. Inset: Cyclic voltammograms measured at 20 mV s^{-1} for 'bare' (broken line) and PioA coated (continuous line) indium tin oxide electrode. Both experiments performed in 50 mM HEPES, 300 mM NaCl, pH 7.4.

The high potential hemes of PioA have His/Met and His/H_2O ligation. Further insight into the nature of the PioA hemes was gained from the electronic absorbance displayed by solutions of the protein prepared in different oxidation states (Figure 5A). For these experiments we compared the spectral properties of solutions containing PioA equilibrated with air, an excess of the mild reductant ascorbate and an excess of the strong reductant dithionite.

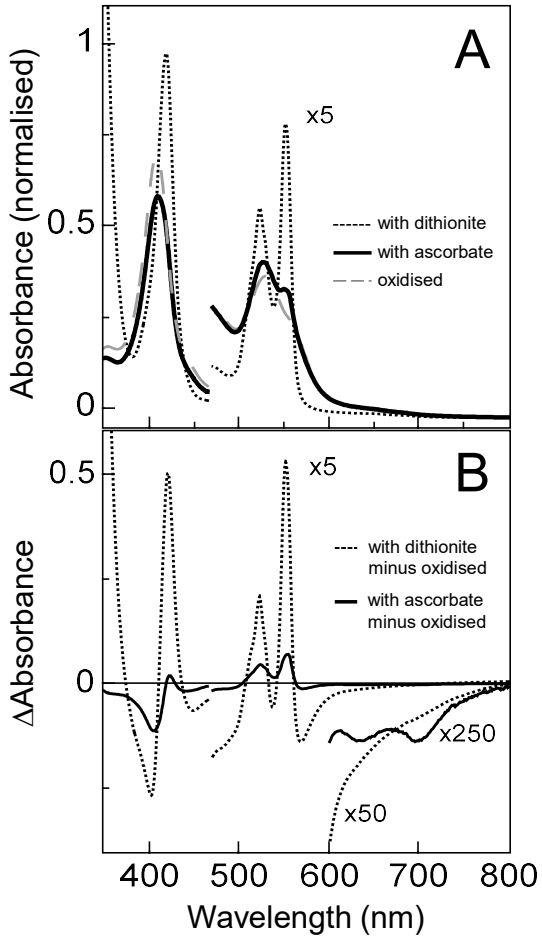

Figure 5. Electronic absorbance of PioA. (A) Spectra of the oxidised (grey dashed), ascorbate reduced (black continuous) and dithionite reduced (black dotted) states. (**B**) Difference spectra for ascorbate reduced minus oxidised states (black continuous) and dithionite reduced minus oxidised states (black dotted). Samples in 50 mM HEPES, 300 mM NaCl, pH 7.4 for PioA concentrations of 7.4 μM (> 460 nm) and 0.7 μM (< 460 nm). Absorbance normalised to that of the lower concentration sample.

Solutions of air-oxidised PioA displayed spectral features typical of oxidised *c*-type hemes and indistinguishable from those of the adsorbed protein; a Soret-band maximum at 407 nm with a broad α-/β-band between approx. 500 and 600 nm. After equilibration with excess ascorbate the solution potential is approx. +60 mV [33] and the electronic absorbance is changed. A smaller, broader Soret band and two small sharp peaks in the α-/β-band are indicative of approx. 13% heme reduction. Thus, the redox

properties of PioA solutions are comparable to those of the protein adsorbed on conductive metal oxide electrodes (Figure 4).

For certain ligand sets Fe(III), but not Fe(II), hemes display ligand-to-metal charge-transfer bands between 600 and 750 nm at energies indicative of the chemical nature of their axial ligands [34]. In this spectral window the difference spectrum (Figure 5B) for ascorbate reduced minus oxidised PioA reveals two negative features. The trough centred at 630 nm is indicative of reduction of high-spin Fe(III) heme(s) most likely having His/H_2O ligation. The trough centred at 700 nm is indicative of reduction of low-spin Fe(III) heme(s) with His/Met ligation. We conclude that oxidised PioA contains His/H_2O and His/Met ligated hemes that are (partially) reduced by addition of ascorbate.

Addition of an excess of the strong reducing agent dithionite produces a solution potential of approx. -500 mV [35] and spectral features indicative of fully reduced PioA (Figure 5A). The Soret band maximum is at 419 nm and well-defined α-/β-band maxima are present at 552 and 523 nm respectively. In the difference spectrum for dithionite-reduced minus oxidised PioA no clear features were distinguished above 600 nm (Figure 5B). Instead a broad negative feature typical for the reduction of low-spin His/His ligated hemes is dominant.

DISCUSSION

Multiheme cytochromes have evolved to move electrons across cell membranes and extracellular structures over distances exceeding several microns [36]. These remarkable properties have found application in the production of electricity by microbial fuel cells [37] and value-added chemicals during microbial electrosynthesis [38-40] where electrons may flow out from, or into, bacteria. Interest in harnessing the electrical properties of the purified multiheme cytochromes is also increasing. Their conductance can rival that of organic semiconductors and they offer renewable, readily engineered and flexible materials that electronically interface live cells and synthetic materials [36, 41]. For these reasons, and to understand the determinants of biological electron transfer in diverse microorganisms, it is of interest to resolve structural and electronic properties of multiheme cytochromes from different bacterial species. Insights into these structure-function relationships are readily available from multi-disciplinary studies that combine electrochemical, spectroscopic and structural methods, e.g. [7, 9, 26, 42, 43]. In this work we used such an approach to provide the first detailed account of the structure-function relationship for PioA. We find that PioA, which has evolved to transfer electrons across the bacterial outer membrane and into *R. palustris* TIE-1, differs in several properties from the homologous MtrA protein, which has evolved to transfer electrons out from *Shewanella* species.

The relatively well-studied outer membrane spanning MtrA protein of *Shewanella* species has His/His ligation of all ten-hemes [11]. By contrast this study has revealed His/Met and His/H_2O ligated hemes in the outer membrane spanning PioA cytochrome of *R. palustris* TIE-1. Similarly ligated hemes are also present in the nonaheme cytochrome OcwA that participates in extracellular electron transfer by the Gram-positive *Thermincola potens* JR [32]. MtrA and PioA have high sequence similarity, including the distribution of ten CxxCH *c*-heme binding motifs (Figure 6A). Combining this information with the X-

ray structure of *S. baltica* OS185 MtrA [11] we are able to present a structural model for PioA (Figure 6B) that provides molecular-level insight into the origin of differences between the MtrA and PioA cytochromes. The model has a chain of ten hemes spanning the longest dimension of PioA (Figure 6B). The hemes are arranged in order of the CxxCH binding motifs to which they are attached, such that the chain extends from N-terminal Heme 1 to C-terminal Heme 10. Neighbouring hemes sit in close proximity and alternate in having configurations of perpendicular and parallel porphyrin ring planes. The model is validated by hydrodynamic modelling of MtrA (90 Å × 39 Å × 45 Å) using SOMO [44] that predicts a sedimentation coefficient of 2.85 S, a value similar to that measured here for PioA (2.94 S). In addition, the MtrA model has a f/f_0 ratio of 1.30, close to the value of 1.33 measured for PioA.

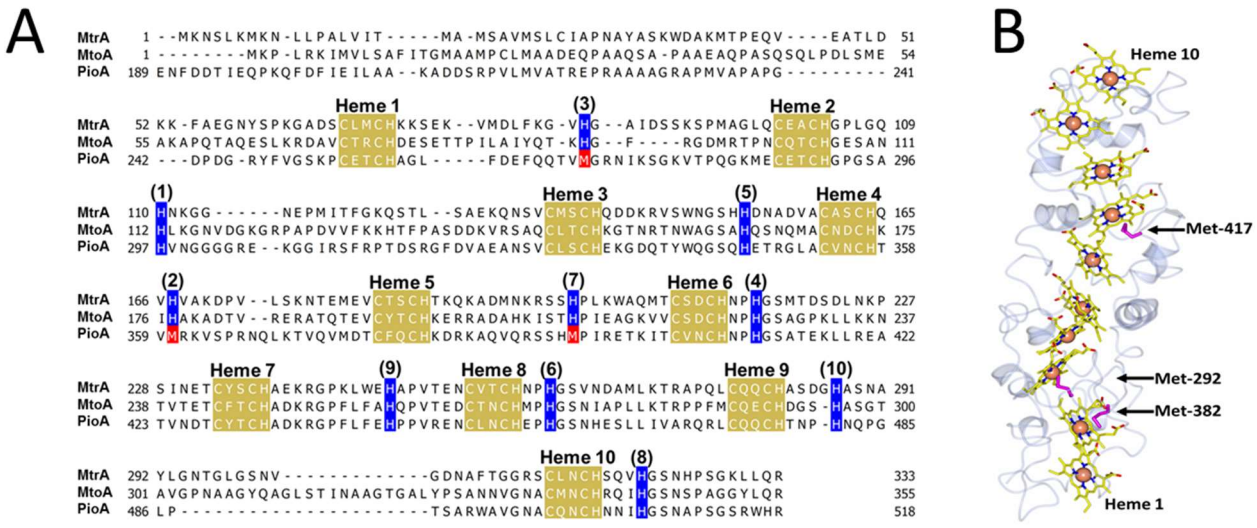

Figure 6. Predicted heme ligation of PioA from *R. palustris* TIE-1. (A) Sequence alignment of *Shewanella baltica* OS185 MtrA, *Sideroxydans lithotrophicus* ES-1 MtoA and the sequence corresponding to the processed *Rhodopseudomonas palustris* TIE-1 PioA produced by Clustal Omega [45] and edited in Jalview [46]. *c*-Type heme binding motifs are highlighted in gold and labelled based upon their position within the amino acid sequence. Known distal histidines of MtrA [11] and predicted distal histidines of MtoA and PioA are highlighted in blue. Predicted distal methionines of PioA are shown in red. The corresponding heme of the distal ligands, as determined from the structure of MtrA, are given in parentheses. **(B)** Homology model of PioA produced by Phyre 2 [47] using MtrA from *S. baltica* OS185 as a template [11]. The protein is shown in blue cartoon representation and the hemes are shown in yellow stick representation. Methionines which may potentially form distal ligands to Hemes 2, 3 and 7 are labelled and shown in pink stick representation.

PioA hemes receive proximal ligation by His of the corresponding CxxCH *c*-heme binding motifs. Of the ten distal His ligands identified in the crystal structure of *S. baltica* MtrA it is significant that only seven are conserved in PioA (Figure 6A). These conserved His residues are the most likely distal ligands

of the corresponding PioA sites, namely, Hemes 1, 4, 5, 6, 8, 9 and 10. The distal His ligands to Hemes 2, 3 and 7 are not conserved and Met is found in place of the corresponding residues, at positions 382, 292 and 417 respectively (Figure 6). Thus, Hemes 2, 3 and/or 7 are candidates for the His/Met ligated PioA heme(s) identified in this study. We note that for Heme 7, the predicted distal ligand of Met417 is preceded by His416 which could also ligate this heme.

All ten distal His ligands of MtrA are conserved in the sequence of another MtrA-family member, MtoA of *S. lithotrophicus* (Figure 5A). Like MtrA and PioA, MtoA is associated with the bacterial outer membrane [9]. Like PioA, and in contrast to MtrA, MtoA naturally participates in electron uptake following Fe(II) oxidation (Figure 1A). Thus, there is no indication that His/Met ligation alone distinguishes decaheme cytochromes with a primary role passing electrons into, rather than out from, bacteria. Nevertheless, it is clear that His/Met ligation contributes to PioA having redox activity at potentials more positive than MtoA and MtrA (Figure 7). It is possible that the His/Met ligated PioA hemes store electrons from Fe(II) oxidation prior to delivery to the periplasmic PioC protein (reduction potential ≈+450 mV [48]) that is proposed [48] as the immediate donor to the reaction centre located in the inner membrane (Figure 1A right). Full details of the electron transfer pathway and enzymology of carbon-fixation in *R. palustris* TIE-1 can be found in the studies of Guzman *et al* [12] and Bird *et al* [48].

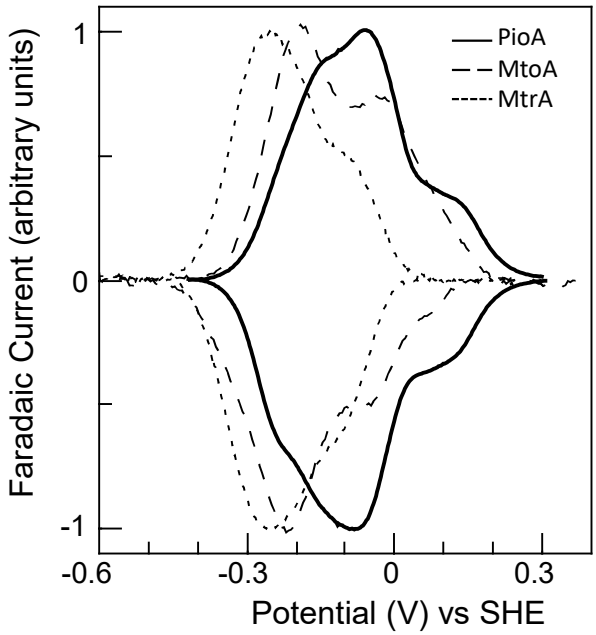

Figure 7. Cyclic voltammograms compared for adsorbed electroactive PioA (continuous), MtoA (dashed) and MtrA (dotted). pH 7. Scan rate 50 mV s^{-1}.

The crystal structure of the *S. baltica* MtrA:MtrB complex shows MtrA Heme 10 presented on the cell surface and Hemes 1 and 2 presented to the periplasm [11]. If PioB wraps PioA in a similar manner, which seems likely, there will be little opportunity for the His/Met ligated hemes to participate in direct electron exchange with extracellular redox partners, soluble Fe(II) or electrodes. If Heme 10 is presented to the external environment it is tempting to suggest His/H_2O ligation at this site to allow close approach of

soluble Fe(II) complexes that may facilitate their oxidation. From sequence analysis, another candidate for His/H_2O ligation is Heme 7. This species could exist as an intermediate if exchange of His416 and Met417 as distal ligands occurs. We note that the MtrA hemes have reduction potentials between approximately 0 and -400 mV (Figure 7 [7]). Thus, we predict very little reduction of MtrA will occur when that protein is equilibrated with excess of the mild-reductant ascorbate. Because the MtrA crystal structure defines ten hemes with His/His ligation, we do not expect to see charge transfer bands indicative of His/Met or His/water ligated hemes in the electronic absorbance of MtrA.

The properties of PioA revealed in this study are significant for anticipating the corresponding features of the PioA-homologs predicted in a number of other species (e.g. Figure 1 and Figure S1). A first defining feature of the PioA-family is cleavage of approximately 240 residues from the N-terminus that results in mature decaheme cytochromes of ≈40 kDa. This is shown here, and previously [19], for PioA of *R. palustris* TIE-1 and has been reported for the PioA proteins of *R. vannielii* DSM 162 and *R. udaipurense* JA643 [19]. Sequence analysis shows the potential for His/Met ligation of Heme 2 in decaheme PioA homologs from over 30 different bacterial genera (Figure S7). The adjacent His-Met pair of amino acids at the sequence position corresponding to the distal ligand of Heme 7 is also conserved in these homologs. His/Met ligation of Heme 3 is less common and appears to be primarily associated with PioA homologs from purple non-sulphur bacteria belonging to the alphaproteobacteria class. Thus, we propose the presence of His-Met ligated hemes is a second defining feature of the PioA-family that distinguishes them from the more widely studied MtrA-family.

From the perspective of biotechnology our results are significant in expanding knowledge of the molecular basis of microbial electrochemistry [5, 6, 37-40, 49]. The well-studied MtrA proteins have a natural role in electron export from *Shewanella* species and bacterial oxidation at anodes (Figure 1A left). By contrast PioA from *R. palustris* TIE-1 has evolved to allow electron uptake for bacterial light-driven carbon fixation (Figure 1A right). This process provides inspiration for strategies to synthesize valuable chemicals while reducing our reliance on fossil reserves and removing a potent greenhouse gas. *R. palustris* TIE-1 is genetically tractable [12, 19]. However, to the best of our knowledge it has not yet been engineered for microbial electrosynthesis through light-driven CO_2-reduction. Such engineering is likely to require that electron transfer from cathodes to photosynthetic reaction centres is uncoupled from downstream pathways that are naturally optimised to use the photoenergised electrons for biomass production. Such an approach could circumvent the low current densities displayed by *R. palustris* TIE-1 which are typical for microbial electrosynthesis and presumed to be limited by the rate of biomass production [12, 16-18, 38]. An alternate approach to enhanced microbial electrosynthesis would engineer an efficient conduit for electron uptake into a chassis microorganism developed for the desired chemical synthesis. The properties of PioA described here provide the first molecular details necessary for rational engineering of such a conduit in bacterial outer membranes.

Experimental Procedures

Bacterial Strains, Plasmids and Strains: The gene encoding PioA from *R. palustris* TIE-1 (*1623 bp, Rpal_0817*) was codon optimised for expression in *S. oneidensis* MR-1 and additional base pairs introduced to encode for a C-terminal Strep II tag (WSHPQFEK) to aid purification. Additional base pairs encoding a stop codon and a ribosome binding site were included at the 5' end of the gene to aid overexpression when subcloned into the pBAD202/D-TOPO expression vector. The corresponding gene was amplified from plasmid pEX-K4*_pioA* (Eurofins Genomics) and cloned into pBAD202 utilizing a directional TOPO cloning kit (Invitrogen). The resulting vector, pBAD202*_pioA*, was transformed by electroporation into *Shewanella oneidensis* strain MR-1 and a variant lacking the *mtr* operon (LS527) [9] to give recombinant strains MR-1*_pioA* and Δ*mtr_pioA*, respectively. Full details of the gene sequence and the primers for PCR amplification are provided in the Supporting Information (Figure S2).

Protein Purification: Recombinant strain MR-1*_pioA* was cultured anaerobically at 30 °C in M72 medium (Casein digest peptone 15 g L^{-1}, papaic digest of soybean meal 5 g L^{-1}, NaCl 5 g L^{-1}) supplemented with 20 mM sodium lactate, 30 mM sodium fumarate and 20 mM HEPES (each from a 200 mM stock solution at pH 8) and containing 50 μg mL^{-1} kanamycin. Induction in mid-exponential growth (OD_{600} 0.4-0.6) was by addition of 5 mM L-arabinose. Cells were harvested 6 hours later by centrifugation (20 min, 7500× *g*, 4 ºC), washed and resuspended in 50 mM sodium phosphate, 300 mM NaCl, pH 8.0 (Buffer A). After addition of SigmaFAST protease inhibitor, 1 mM dithiothreitol and DNase the cells were lysed by three passes through a French Press (16,000 psi). After addition (0.1% by volume) of biotin blocking buffer (IBA Solutions for Lifesciences), cell debris and unbroken cells were pelleted by centrifugation (30 min, 5500 × *g*, 4ºC). The supernatant was recovered and subjected to centrifugation (60 min, 185000 × *g*, 4ºC) to pellet the membrane fraction. Purification of PioA was from the soluble fraction (supernatant) and was monitored by electronic absorbance spectroscopy and SDS-PAGE; for the latter, proteins were visualized by Coomassie stain and peroxidase-linked heme stain employing 3-3′-5-5′ tetramethylbenzidine. Soluble cell lysate was applied to a 5 ml Strep-Tactin XT Superflow Column (IBA Solutions for Lifesciences) equilibrated with Buffer A. After washing with Buffer A, bound protein was eluted with 40 mM biotin in Buffer A and applied to a Superose 6 Increase 10/300GL preparative grade gel filtration column equilibrated with 50 mM HEPES, 300 mM NaCl, pH 8.0. Eluted protein (A_{409}/A_{280} = 4.7) was concentrated and exchanged into 50 mM HEPES, 300 mM NaCl, pH 7.4 (Buffer B) using a centrifugal concentrator (3 kDa MWCO, PES, Pierce™). Aliquots of the purified protein were flash-frozen in liquid nitrogen and stored at -80 ºC until required.

Biochemical Analyses: LC-MS was performed as described previously [50] with PioA (typically 1 mg mL^{-1}) diluted with formic acid (0.1% v/v) and acetonitrile (2% v/v) prior to analysis. Thiol(ate) was quantified using the Measure-iT™ Thiol Assay kit (Invitrogen) following the manufacturer's protocol with samples incubated at 37 ºC for 30 min before spectroscopy; reduced glutathione produced the calibration curve and the fluorescence intensity at 517 nm was quantified for excitation at 494 nm. Protein

concentration (mg mL^{-1}) was quantified with BCA reagent (BioRad) using bovine serum albumin as the standard. Pyridine-hemochrome analysis was performed as described [24].

***Analytical Ultracentrifugation*:** Sedimentation equilibrium and sedimentation velocity were performed using a Beckman Optima XLA-I analytical ultracentrifuge equipped with scanning absorbance optics. Measurements were performed in Buffer B for which the density and viscosity were calculated as 1.0144 g/mL and 1.0611×10^{-2} P respectively using Sedenterp software [25]. A partial specific volume (0.7347 mL g^{-1}) was calculated from the amino acid sequence of truncated PioA using the utility software in Ultrascan II software [51]. Sedimentation equilibrium was performed at 20 °C using speeds of 15k, 18k, and 21k rpm with absorbance profiles recorded at 409 nm (0.5 μM PioA) or 520 nm (5 μM PioA). Sedimentation equilibrium profiles were analysed with the programme Ultrascan II.

Sedimentation velocity was conducted at 20 °C and 40k rpm with 0.8 μM PioA in 50 mM HEPES, 300 mM NaCl, pH 7.4. Absorbance was recorded at 409 nm every 2 minutes. Following both experiments, the samples were removed and SDS-PAGE gels stained for heme showed no evidence for PioA degradation. Data were fitted using the *c*(s) distribution analysis in the software SEDFIT [52]. The molecular weight *M* of PioA was obtained from the Svedberg equation, $\frac{S}{D} = \frac{M(1-\bar{\nu}\rho)}{RT}$ [25], where *S* is the PioA sedimentation coefficient; *D* the PioA diffusion coefficient; $\bar{\nu}$ the PioA partial specific volume, ρ the solvent buffer density, *R* the gas constant and *T* the temperature.

Electrochemistry: Spectro-potentiometry and cyclic voltammetry were performed by direct protein electrochemistry using three-electrode cell configurations and an Autolab PGSTAT30 potentiostat (EcoChemie) controlled by NOVA software. For cyclic voltammetry the cell was inside a Faraday cage situated in a N_2-chamber as previously described [53]. Potentiometric titration of PioA monitored by electronic absorbance spectroscopy was performed with the protein adsorbed on optically transparent mesoporous nanocrystalline SnO_2 electrodes. Electrodes were prepared by covering them with ice-cold solutions of PioA (17 μM) and the coadsorbate neomycin (25 mM) in Buffer B. After approximately 20 min the electrode was rinsed with Buffer B, to remove loosely-bound material, and mounted in an optical cuvette filled with anaerobic Buffer B and fitted with reference and counter electrodes as previously described [26]. Adsorbed PioA at ambient temperature was equilibrated at defined potentials and the electronic absorbance recorded. Spectral quality was optimised by mounting an equivalent electrode, lacking adsorbed protein, in the reference beam to minimise contributions from light scattering by the electrode. Protein film cyclic voltammetry was performed with PioA (17 μM) and the coadsorbate neomycin (25 mM) adsorbed on hierarchical indium tin oxide electrodes (750 nm macropore size, ~50 nm mesoporous features, 20 μm film thickness, 0.25 cm^2 geometrical surface area [42]) placed in solutions at 20 °C containing 300 mM NaCl and 50 mM of either Bis-Tris (pH 6.4), HEPES (pH 7.4), or CHES (pH 9.4) for the indicated solution pH.

Bioinformatics: A BLAST [54] search was utilized to identify decaheme homologs of PioA, resulting in 773 protein sequences being retrieved. CxxCH motifs and their sequence locations were identified utilizing ScanProsite.[55] Signal peptides and predicted cleavage sites were identified utilizing SignalP 5.0.[56] Sequences were aligned and phylogenetic trees calculated utilizing Clustal Omega [57]. Phylogenetic trees/Cladograms were formatted and protein features mapped using iTOL.[58]

Acknowledgments: We thank Prof. James Durrant (Imperial College, London) for generous provision of optically transparent SnO_2 electrodes. Funding was from the UK Biotechnology and Biological Sciences Research Council (BB/L022176, BB/P01818X, BB/S002499 to J.N.B. and T.A.C. and a Norwich Research Park Biosciences Doctoral Training Partnership PhD studentship to S.E.H.P.) and Engineering and Physical Sciences Research Council (DTA Ph.D. studentship to K.P.S.). D.L. is grateful to the Collaborative Innovation Center of Suzhou Nano Science and Technology (NANO-CIC) and the Chinese Collaborative Academic Training Program for Post-doctoral Fellows. J.N.B. acknowledges a Royal Society Leverhulme Trust Senior Research Fellowship.

Conflict of interest: The authors declare that they have no conflicts of interest with the contents of this article.

REFERENCES

[1] Ilbert M and Bonnefoy V 2013 Insight into the evolution of the iron oxidation pathways *Biochim. Biophys. Acta* **1827** 161-75

[2] Bird L J, Bonnefoy V, and Newman D K 2011 Bioenergetic challenges of microbial iron metabolisms *Trends Microbiol.* **19** 330-40

[3] Melton E D, Swanner E D, Behrens S, Schmidt C, and Kappler A 2014 The interplay of microbially mediated and abiotic reactions in the biogeochemical Fe cycle *Nat. Rev. Microbiol.* **12** 797-808

[4] He S M, Barco R A, Emerson D, and Roden E E 2017 Comparative genomic analysis of neutrophilic iron(II) oxidizer genomes for candidate genes in extracellular electron transfer *Front. Microbiol.* **8** doi: 10.3389/fmicb.2017.01584

[5] Shi L, Dong H L, Reguera G, Beyenal H, Lu A H, Liu J, Yu H Q, and Fredrickson J K 2016 Extracellular electron transfer mechanisms between microorganisms and minerals *Nat. Rev. Microbiol.* **14** 651-62

[6] White G, Edwards M, Gomez-Perez L, Richardson D, Butt J, and Clarke T 2016 Mechanisms of bacterial extracellular electron exchange *Adv. Microb. Physiol.* **68** 87-138

[7] Hartshorne R S, Reardon C L, Ross D, Nuester J, Clarke T A, Gates A J, Mills P C, Fredrickson J K, Zachara J M, Shi L, Beliaev A S, Marshall M J, Tien M, Brantley S, Butt J N, and Richardson D J 2009 Characterization of an electron conduit between bacteria and the extracellular environment *Proc. Natl. Acad. Sci. USA* **106** 22169-74

[8] White G F, Shi Z, Shi L, Wang Z M, Dohnalkova A C, Marshall M J, Fredrickson J K, Zachara J M, Butt J N, Richardson D J, and Clarke T A 2013 Rapid electron exchange between surface-exposed bacterial cytochromes and Fe(III) minerals *Proc. Natl. Acad. Sci. USA* **110** 6346-51

[9] Liu J, Wang Z M, Belchik S M, Edwards M J, Liu C X, Kennedy D W, Merkley E D, Lipton M S, Butt J N, Richardson D J, Zachara J M, Fredrickson J K, Rosso K M, and Shi L 2012 Identification and characterization of MtoA: a decaheme c-type cytochrome of the neutrophilic Fe(II)-oxidizing bacterium *Sideroxydans lithotrophicus* ES-1 *Front. Microbiol.* **3** doi: 10.3389/fmicb.2012.00037

[10] Liu Y M, Wang Z M, Liu J, Levar C, Edwards M J, Babauta J T, Kennedy D W, Shi Z, Beyenal H, Bond D R, Clarke T A, Butt J N, Richardson D J, Rosso K M, Zachara J M, Fredrickson J K, and

Shi L 2014 A trans-outer membrane porin-cytochrome protein complex for extracellular electron transfer by *Geobacter sulfurreducens* PCA *Environ. Microbiol. Rep.* **6** 776-85
[11] Edwards M J, White G F, Butt J N, Richardson D J, and Clarke T A 2019 The structure of a biological insulated transmembrane molecular wire *Cell* preprint: 10.2139/ssrn.3445677
[12] Guzman M S, Rengasamy K, Binkley M M, Jones C, Ranaivoarisoa T O, Singh R, Fike D A, Meacham J M, and Bose A 2019 Phototrophic extracellular electron uptake is linked to carbon dioxide fixation in the bacterium *Rhodopseudomonas palustris Nat. Commun.* **10** doi:10.1038/s41467-019-09377-6
[13] Fredrickson J K, Romine M F, Beliaev A S, Auchtung J M, Driscoll M E, Gardner T S, Nealson K H, Osterman A L, Pinchuk G, Reed J L, Rodionov D A, Rodrigues J L M, Saffarini D A, Serres M H, Spormann A M, Zhulin I B, and Tiedje J M 2008 Towards environmental systems biology of *Shewanella Nat. Rev. Microbiol.* **6** 592-603
[14] Jiao Y and Newman D K 2007 The *pio* operon is essential for phototrophic Fe(II) oxidation in *Rhodopseudomonas palustris* TIE-1 *J. Bacteriol.* **189** 1765-73
[15] Larimer F W, Chain P, Hauser L, Lamerdin J, Malfatti S, Do L, Land M L, Pelletier D A, Beatty J T, Lang A S, Tabita F R, Gibson J L, Hanson T E, Bobst C, Torres J L T Y, Peres C, Harrison F H, Gibson J, and Harwood C S 2004 Complete genome sequence of the metabolically versatile photosynthetic bacterium *Rhodopseudomonas palustris Nat. Biotechnol.* **22** 55-61
[16] Bose A, Gardel E J, Vidoudez C, Parra E A, and Girguis P R 2014 Electron uptake by iron-oxidizing phototrophic bacteria *Nat. Commun.* **5** doi:10.1038/ncomms4391
[17] Rengasamy K, Ranaivoarisoa T, Singh R, and Bose A 2018 An insoluble iron complex coated cathode enhances direct electron uptake by *Rhodopseudomonas palustris* TIE-1 *Bioelectrochem.* **122** 164-73
[18] Doud D F R and Angenent L T 2014 Toward electrosynthesis with uncoupled extracellular electron uptake and metabolic growth: enhancing current uptake with *Rhodopseudomonas palustris Environ. Sci. Technol. Lett.* **1** 351-55
[19] Gupta D, Sutherland M C, Rengasamy K, Meacham J M, Kranz R G, and Bose A 2019 Photoferrotrophs produce a PioAB electron conduit for extracellular electron uptake. *mBIO* **10** e02668-19
[20] Edwards M J, Baiden N A, Johs A, Tomanicek S J, Liang L Y, Shi L, Fredrickson J K, Zachara J M, Gates A J, Butt J N, Richardson D J, and Clarke T A 2014 The X-ray crystal structure of *Shewanella oneidensis* OmcA reveals new insight at the microbe-mineral interface *FEBS Lett.* **588** 1886-90
[21] Edwards M J, White G F, Norman M, Tome-Fernandez A, Ainsworth E, Shi L, Fredrickson J K, Zachara J M, Butt J N, Richardson D J, and Clarke T A 2015 Redox linked flavin sites in extracellular decaheme proteins Involved in microbe-mineral electron transfer *Sci. Rep.* **5** doi:10.1038/srep11677
[22] Beckwith C R, Edwards M J, Lawes M, Shi L, Butt J N, Richardson D J, and Clarke T A 2015 Characterization of MtoD from *Sideroxydans lithotrophicus:* a cytochrome *c* electron shuttle used in lithoautotrophic growth *Front. Microbiol.* **6** doi: 10.3389/fmicb.2015.00332
[23] Abboud R, Popa R, Souza-Egipsy V, Giometti C S, Tollaksen S, Mosher J J, Findlay R H, and Nealson K H 2005 Low-temperature growth of *Shewanella oneidensis* MR-1 *Appl. Environ. Microbiol.* **71** 811-16
[24] Barr I and Guo F 2015 Pyridine hemochromagen assay for determining the concentration of heme in purified protein solutions *Bio Protoc.* **5** e1594
[25] Laue T, Shah B D, Ridgeway T M, and Pelletier S L, Computer-aided interpretation of analytical sedimentation data for proteins, in Analytical ultracentrifugation in biochemistry and polymer science, Harding S E R A J, Horton J C, Editor. 1992, Royal Society of Chemistry: Cambridge, UK. 90-125.
[26] Marritt S J, Kemp G L, Xiaoe L, Durrant J R, Cheesman M R, and Butt J N 2008 Spectroelectrochemical characterization of a pentaheme cytochrome in solution and as electrocatalytically active films on nanocrystalline metal-oxide electrodes *J. Am. Chem. Soc.* **130** 8588-89
[27] Ioannidis L A, Nikolaou P, Panagiotopoulos A, Vassi A, and Topoglidis E 2019 Microperoxidase-11 modified mesoporous SnO_2 film electrodes for the detection of antimalarial drug artemisinin *Anal. Methods* **11** 3117-25

[28] Mersch D, Lee C Y, Zhang J Z, Brinkert K, Fontecilla-Camps J C, Rutherford A W, and Reisner E 2015 Wiring of photosystem II to hydrogenase for photoelectrochemical water splitting *J. Am. Chem. Soc.* **137** 8541-49
[29] Fang X, Sokol K P, Heidary N, Kandiel T A, Zhang J Z, and Reisner E 2019 Structure-activity relationships of hierarchical three-dimensional electrodes with photosystem II for semiartificial photosynthesis *Nano Lett.* **19** 1844-50
[30] Doyle R M A S, Richardson D J, Clarke T A, and Butt J N 2013 Freely diffusing versus adsorbed protein: Which better mimics the cellular state of a redox protein? *Electrochim. Acta* **110** 73-78
[31] Hartshorne R S, Jepson B N, Clarke T A, Field S J, Fredrickson J, Zachara J, Shi L, Butt J N, and Richardson D J 2007 Characterization of *Shewanella oneidensis* MtrC: a cell-surface decaheme cytochrome involved in respiratory electron transport to extracellular electron acceptors *J. Biol. Inorg. Chem.* **12** 1083-94
[32] Costa N L, Hermann B, Fourmond V, Faustino M M, Teixeira M, Einsle O, Paquete C M, and Louro R O 2019 How thermophilic Gram-positive organisms perform extracellular electron transfer: characterization of the cell surface terminal reductase OcwA *MBio* **10** DOI: 10.1128/mBio.01210-19
[33] Jenner L P, Kurth J M, van Helmont S, Sokol K P, Reisner E, Dahl C, Bradley J M, Butt J M, and Cheesman M R 2019 Heme ligation and redox chemistry in two bacterial thiosulfate dehydrogenase (TsdA) enzymes *J. Biol. Chem.* **294** 18002-14
[34] Cheesman M R, Watmough N J, Gennis R B, Greenwood C, and Thomson A J 1994 Magnetic-circular-dichroism studies of *Escherichia coli* cytochrome *bo* - Identification of high-spin ferric, low-spin ferric and ferryl [Fe(IV)] forms of heme *o Eur. J. Biochem.* **219** 595-602
[35] Mayhew S G 1978 Redox potential of dithionite and SO_2^- from equilibrium reactions with flavodoxins, methyl viologen and hydrogen plus hydrogenase *Eur. J. Biochem.* **85** 535-47
[36] Ing N L, El-Naggar M Y, and Hochbaum A I 2018 Going the distance: long-range conductivity in protein and peptide bioelectronic materials *J. Phys. Chem. B* **122** 10403-23
[37] Gul M M and Ahmad K S 2019 Bioelectrochemical systems: Sustainable bio-energy powerhouses *Biosens. Bioelectron.* **142** 11576
[38] Rengasamy K, Singh R, and Bose A 2019 Microbial electron uptake in microbial electrosynthesis: a mini-review *J. Ind. Microbial. Biotechnol.* **46** 1419-26
[39] Kracke F, Vassilev I, and Kromer J O 2015 Microbial electron transport and energy conservation - the foundation for optimizing bioelectrochemical systems *Front. Microbiol.* **6** doi:10.3389/fmicb.2015.00575
[40] Su L and Ajo-Franklin C M 2019 Reaching full potential: bioelectrochemical systems for storing renewable energy in chemical bonds. *Curr. Opinion. Biotechnol.* **57** 66-72
[41] Garg K, Ghosh M, Eliash T, van Wonderen J H, Butt J N, Shi L, Jiang X Y, Zdenek F, Blumberger J, Pecht I, Sheves M, and Cahen D 2018 Direct evidence for heme-assisted solid-state electronic conduction in multi-heme *c*-type cytochromes *Chem. Sci.* **9** 7304-10
[42] Reuillard B, Ly K H, Hildebrandt P, Jeuken L J C, Butt J N, and Reisner E 2017 High performance reduction of H_2O_2 with an electron transport decaheme cytochrome on a porous ITO electrode *J. Am. Chem. Soc.* **139** 3324-27
[43] Marritt S J, Lowe T G, Bye J, McMillan D G G, Shi L, Fredrickson J, Zachara J, Richardson D J, Cheesman M R, Jeuken L J C, and Butt J N 2012 A functional description of CymA, an electron-transfer hub supporting anaerobic respiratory flexibility in Shewanella *Biochem. J.* **444** 465-74
[44] Rai N, Nollmann M, Spotorno B, Tassara G, Byron O, and Rocco M 2005 SOMO(SOlution MOdeler): Differences between X-ray- and NMR-derived bead models suggest a role for side chain flexibility in protein hydrodynamics *Structure* **13** 723-34
[45] Madeira F, Park Y M, Lee J, Buso N, Gur T, Madhusoodanan N, Basutkar P, Tivey A R N, Potter S C, Finn R D, and Lopez R 2019 The EMBL-EBI search and sequence analysis tools APIs in 2019 *Nucleic Acids Res.* **47** W636-W41
[46] Waterhouse A M, Procter J B, Martin D M A, Clamp M, and Barton G J 2009 Jalview Version 2-a multiple sequence alignment editor and analysis workbench *Bioinformatics* **25** 1189-91
[47] Kelley L A, Mezulis S, Yates C M, Wass M N, and Sternberg M J E 2015 The Phyre2 web portal for protein modeling, prediction and analysis *Nat. Protoc.* **10** 845-58
[48] Bird L J, Saraiva I H, Park S, Calcada E O, Salgueiro C A, Nitschke W, Louro R O, and Newman D K 2014 Nonredundant roles for cytochrome c_2 and two high-potential iron-sulfur proteins in the photoferrotroph *Rhodopseudomonas palustris* TIE-1 *J. Bacteriol.* **196** 850-58

[49] Costa N L, Clarke T A, Philipp L A, Gescher J, Louro R O, and Paquete C M 2018 Electron transfer process in microbial electrochemical technologies: The role of cell-surface exposed conductive proteins *Bioresour. Technol.* **255** 308-17
[50] van Wonderen J H, Li D B, Piper S E H, Lau C Y, Jenner L P, Hall C R, Clarke T A, Watmough N J, and Butt J N 2018 Photosensitised multiheme cytochromes as light-driven molecular wires and resistors *ChemBioChem* **19** 2206-15
[51] Demeler B, UltraScan - A comprehensive data analysis software package for analytical ultracentrifugation experiments in Analytical Ultracentrifugation: Techniques and Methods. , Scott D J, Harding S E, and Rowe A J, Editors. 2005, Royal Society of Chemistry: Cambridge, UK. 210-29.
[52] Schuck P 2000 Size-distribution analysis of macromolecules by sedimentation velocity ultracentrifugation and Lamm equation modeling *Biophys. J.* **78** 1606-19
[53] Anderson L J, Richardson D J, and Butt J N 2001 Catalytic protein film voltammetry from a respiratory nitrate reductase provides evidence for complex electrochemical modulation of enzyme activity *Biochemistry* **40** 11294-307
[54] Altschul S F, Gish W, Miller W, Myers E W, and Lipman D J 1990 Basic Local Alignment Search Tool *J. Molec. Biol.* **215** 403-10
[55] de Castro E, Sigrist C J A, Gattiker A, Bulliard V, Langendijk-Genevaux P S, Gasteiger E, Bairoch A, and Hulo N 2006 ScanProsite: detection of PROSITE signature matches and ProRule-associated functional and structural residues in proteins *Nucleic Acids Res.* **34** W362-W65
[56] Armenteros J J A, Tsirigos K D, Sonderby C K, Petersen T N, Winther O, Brunak S, von Heijne G, and Nielsen H 2019 SignalP 5.0 improves signal peptide predictions using deep neural networks *Nat. Biotechnol.* **37** 420-23
[57] Sievers F and Higgins D G 2018 Clustal Omega for making accurate alignments of many protein sequences *Protein Sci.* **27** 135-45
[58] Letunic I and Bork P 2016 Interactive tree of life (iTOL) v3: an online tool for the display and annotation of phylogenetic and other trees *Nucleic Acids Res.* **44** W242-W45